universe

Article

Antarctic Survey Telescope 3-3: Overview, System Perfor and Preliminary Observations at Yaoan, Yunnan

Tianrui Sun[1,2], Xiaoyan Li[3], Lei Hu[1], Kelai Meng[1], Zijian Han[3], Maokai Hu[1], Zhengyang L[3], Haikun Wei[3], Fujia Du[3], Shihai Yang[3], Bozhong Gu[3], Xiangyan Yuan[3], Yun Li[3], Huihui Wang[1], Lei Liu[1], Zhenxi Zhu[1], Xuehai Huang[1], Chengming Lei[1], Lifan Wang[4] and Xuefeng Wu[1,2,*]

1 Purple Mountain Observatory, Chinese Academy of Sciences, Nanjing 210023, China; trsun@pmo.ac.cn (T.S.); hulei@pmo.ac.cn (L.H.); mkl@pmo.ac.cn (K.M.); kaihukaihu123@pmo.ac.cn (M.H.); wanghh@pmo.ac.cn (H.W.); lliu@pmo.ac.cn (L.L.); zxzhu@pmo.ac.cn (Z.Z.); xhhuang@pmo.ac.cn (X.H.); cmlei@pmo.ac.cn (C.L.)

2 School of Astronomy and Space Sciences, University of Science and Technology of China, Hefei 230026, China

3 Nanjing Institute of Astronomical Optics & Technology, National Astronomical Observatories, Chinese Academy of Sciences, Nanjing 210042, China; xyli@niaot.ac.cn (X.L.); zjhan@niaot.ac.cn (Z.H.); zyli@niaot.ac.cn (Z.L.); hkwen@niaot.ac.cn (H.W.); fjdu@niaot.ac.cn (F.D.); shyang@niaot.ac.cn (S.Y.); bzhgu@niaot.ac.cn (B.G.); xyyuan@niaot.ac.cn (X.Y.); yli@niaot.ac.cn (Y.L.)

4 George P. and Cynthia Woods Mitchell Institute for Fundamental Physics & Astronomy, Texas A&M University, Department of Physics and Astronomy, 4242 TAMU, College Station, TX 77843, USA; lifan@tamu.edu

* Correspondence: xfwu@pmo.ac.cn

Abstract: The third Antarctic Survey Telescope array instrument at Dome A in Antarctica, the AST3-3 telescope, has been in commissioning from March 2021. We deployed AST3-3 at the Yaoan astronomical station in Yunnan Province for an automatic time-domain survey and follow-up observations with an optimised observation and protection system. The telescope system of AST3-3 is similar to that of AST3-1 and AST3-2, except that it is equipped with a 14 K × 10 K QHY411 CMOS camera. AST3-3 has a field of view of $1.65^{\circ} \times 1.23^{\circ}$ and is currently using the *g* band filter. During commissioning at Yaoan, AST3-3 aims to conduct an extragalactic transient survey, coupled with prompt follow-ups of opportunity targets. In this paper, we present the architecture of the AST3-3 automatic observation system. We demonstrate the data processing of observations by representatives SN 2022eyw and GRB 210420B.

Keywords: wide-field survey; transient observations; robotic optical telescope

Citation: Sun, T.; Li, X.; Hu, L.; Meng, K.; Han, Z.; Hu, M.; Li, Z.; Wen, H.; Du, F.; Yang, S.; et al. Antarctic Survey Telescope 3-3: Overview, System Performance and Preliminary Observations at Yaoan, Yunnan. *Universe* **2022**, *8*, 303. https://doi.org/10.3390/universe8060303

Academic Editor: Luciano Nicastro

Received: 22 April 2022
Accepted: 16 May 2022
Published: 26 May 2022

1. Introduction

In recent years, short time-scale transient sources have become a research hotspot in time-domain astronomy. The time-varying scale of short time-scale transient sources ranges from milliseconds to days and is often associated with violent astrophysical processes, such as supernovae, gravitational wave events, fast radio bursts, gamma-ray bursts, high-energy neutrino events, tidal disruption events of stars. On the one hand, the causes and physical mechanisms of these phenomena still have open questions.They are also observational probes closely related to the frontier of astronomy and physics, such as the verification of general relativity and quantum gravity, dark energy, dark matter, and physics beyond the standard model of particle physics. On the other hand, for transients with short time scales, especially the time-scale of milliseconds to minutes, there is still a lack of systematic observations in the optical waveband. The study of transients requires surveys with a wide field of view (FoV), high photometric precision, and complete time coverage. Large time-domain surveys have developed rapidly in recent years all over the world, such as the Panoramic Survey Telescope And Rapid Response System [1], Zwicky Transient Factory [2,3], Asteroid Terrestrial-impact Last Alert System [4], Gravitational-Wave Optical

Transient Observer [5], Skymapper [6], Deca-Degree Optical Transient Imager [7] and the upcoming Large Synoptic Survey Telescope [8]. In China, large field surveys are also developing rapidly such as the THU-NAOC Transient Survey [9], Tsinghua University-Ma Huateng Telescopes for Survey [10], and China Near-Earth Object Survey [11].

The Antarctica continent possesses very competitive astronomical observation sites because of rare human activities and long astronomical polar nights [12]. Extremely temperature ensures the water vapour content low and stable, thus reducing photometric noise caused by vapour absorption [13]. Atmospheric turbulence on the plateau also reduces the scintillation noise and improves photometric precision [14–16]. In addition, the Antarctic continent has the cleanest air on Earth, with the lowest atmospheric aerosol concentration and negligible artificial light pollution [17]. Dome A is located at the highest point in Antarctica at 77.56° E and 80.36° S , with an elevation of 4093 m ice tap, which has many advantages for astronomical observations [18,19], such as extreme cold temperatures and low absolute humidity on Earth [20–22]. The Antarctic Survey Telescope (AST3) series includes three large FoV and high photometric precision 50/68 cm modified Schmidt telescopes [23,24]. All the three telescopes focus on time-domain astronomy, including variable starts [25–27], exoplanets [28,29], electromagnetic counterparts of gravitational wave events [30,31], and other transients in sky surveys and follow-up observations.

AST3-1 [32] and AST3-2 were installed at Dome A by the 28th and 31st Chinese National Antarctic Research Expeditions in 2012 and 2015. AST3-3 has been in commission since March 2021 at Yaoan astronomical station, in Yunnan Province, China. AST3-3 has an FoV of $1.65^\circ \times 1.23^\circ$, and is currently using the *g*-band filter. In future, AST3-3 will be equipped with a mid-infrared camera, using the unique 2.4 µm *K*-dark infrared window of Dome A to carry out the first Antarctic Infrared Time Domain Astronomy Research Program - Kunlun Infrared Sky Survey (KISS) [33–36].

In the past Observation Run 3 organised by LIGO/Virgo [37], many telescopes were involved in searching for optical counterparts of gravitational wave events. We also searched the GW events with the telescopes of the CHanging Event Survey array at the Yaoan Observatory [38]. Some groups use widely distributed automated telescope arrays to monitor transients, such as the Burst Observer and Optical Transient Exploring System group [39], Télescope à Action Rapide pour les Objets Transitoires [40], COATLI [41,42] and the Mobile Astronomical System of Telescope-Robots [43].

In Section 2, we introduce the weather-based protection system, as well as the network and hardware of the data system. In Section 3, we present the observation procedure and the structure of the observation list to explain the logical sequence of our observations. We also introduce the observation plan of the AST3-3 telescope for both time-domain surveys and targets of opportunities in Section 3. The preliminary results, including data statistics and the observation of gamma-ray burst GRB 210420B are presented in Section 4, and we conclude in Section 5.

2. Observation Hardware

At the beginning of 2021, we placed the AST3-3 telescope into an eight-meter diameter dome as shown in Figure 1 at the Yaoan Astronomical Station at $101^\circ 10^0 47^{00}$ E, $25^\circ 31^0 43^{00}$N, with an elevation of 1900 m in Yunnan Province. The Yaoan station has excellent logistics for supporting the long-term commissioning of telescopes. AST3-3 collaborates with YaoAn High Precision Telescope (YAHPT hereafter, [44]) for multiband follow-up observations of detected transient sources.

The pointing, focusing, and tracking control system of AST3-3 is upgraded from AST3-1 and AST3-2 in Antarctica. The observation computer communicates with the telescope control computer via the local area network based on the TCP/IP protocol with private AST3-3 commands syntax. To avoid cable entanglement of the camera and engines, the reaching time-angle of $\pm$ 180 degrees should be avoided, which indicates that AST3-3 should not observe any object under the north polar axis. With the latitude of Yaoan Station

being 25.5 degrees, the observation limit is set to 30 degrees, which can avoid bad extinction at high zenith angles and the time angle reaching 180 degrees.

Figure 1. AST3-3 deployment in dome.

AST3-3 conducts the time-domain sky survey, follow-up observation for high energy transients and the simultaneous observation of fast radio bursts with the FAST telescope. Different modes of observation require different storage speeds and capacity performances. We built a group of computers with high-speed storage and high-performance servers, as shown in Table 1. The observation computer connects with the camera via optical fibres and an FPGA card for high-speed data swaps. It uses a solid-state-drive with a capacity of 5 Terabytes based RAID-50 systems to capture data as a cache to boost the I/O process, especially in the simultaneous observation of fast radio bursts which requires a short-exposure observation mode. The storage server is constructed with a 220 Terabytes RAID array and a scalable tape library that protects the observation data, processed data and the control database. The pipeline server is built by a high-performance computing server with two 32-core CPUs and two Nvidia A100 (40 GiB) computational cards for data processing. The deep-learning analysis of transient candidates and local area network web hosted in the WebPage server to avoid the crowd of the GPU time in pipeline server. All servers synchronize time to a local GPS server by the network time protocol once per minute.

Table 1. Computer System for AST3-3 in Yaoan Station.

SeverID	Job	Type	CPU and Accelerator	Memory
1	Observation	R7525	AMD 7252 × 2 + FPGA	128 GiB
2	Pipeline	R7525	AMD 7522 × 2 + A100 × 2	512 GiB
3	(NFS) Storage	R740xd2	4214R	128 GiB
4	Asteroid	R740xd2	5118	256 GiB
5	Web	D30	E5-2620	32 GiB

These server computers, housed in a specific room with an air-conditioner, are connected by a 10 GiB Ethernet for data swaps. The uninterruptible power supply (UPS) controller also connects to the local area network to share the status information with all

servers to save data once the power supply fails. Figure 2 shows the intranet structure of the associated control schematics of AST3-3. The software-defined wide-area network (SDWAN) is applied here for remote control and internet security for the whole system.

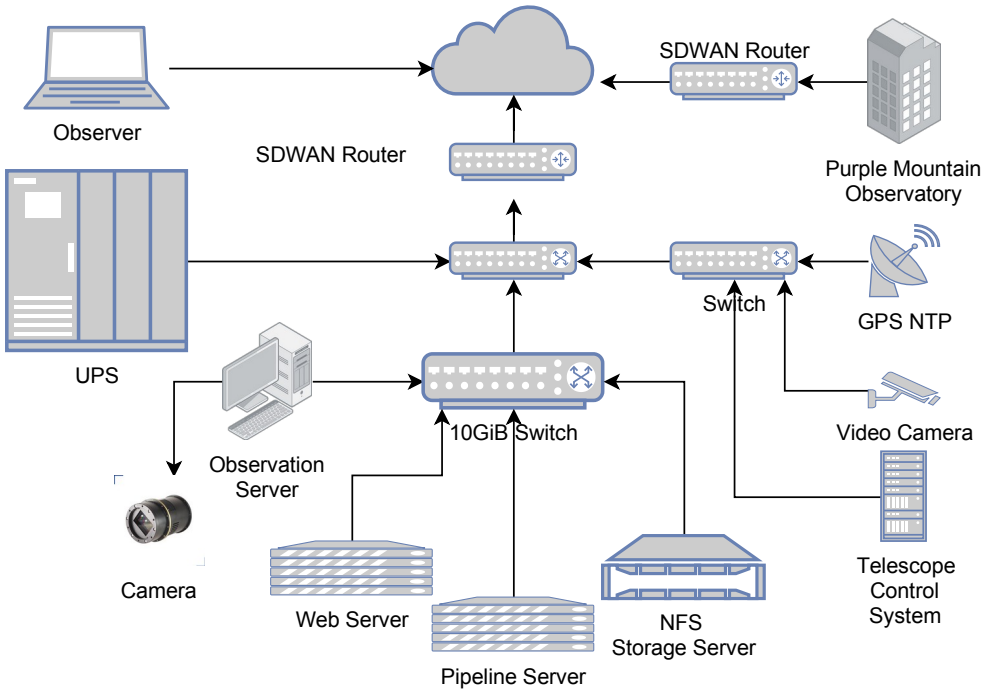

Figure 2. AST3-3 private and local area Internet structure.

2.1. The CMOS Camera

Giving the demand of ultrashort time-scale exposures in the observations of fast radio bursts which could increase the telescope's competitiveness, AST3-3 currently uses a complementary metal-oxide-semiconductor (CMOS) detector camera and an electronic shutter. The AST3-3 is currently equipped with a QHY411 camera, which has a 151 megapixels Sony back-illuminated IMX411 sensor onboard and a dual thermoelectric cooler, satellite clock supports and high-speed fibre connections. This camera sensor has an exposure area of 54 × 40 mm^2 with a physical pixel size of 3.76 × 3.76 μm^2, which contains a 14,304 × 10,748-pixel array. The FoV with this camera is 1.65° × 1.23°, smaller than those on AST3-1 and AST3-2. The electric shutter of this camera accepts an exposure time from 20 μs to 3600 s, which allows both long- and short-exposure observations. The camera provides several different exposure modes, which leads to different gain settings that would cause different system gain, readout noise, and full-wells. Based on the feature datasheet of the camera, in typical observation with readout mode # 4, the gain setting is usually set as 0, obtaining a system gain of 1, readout noise of 3.6 electrons and full-well near 60,000 ADUs.

The camera contains an electronic rolling shutter that introduces the feature of different start and end exposure times for each column. This difference could not occur does not affect the physical results for most long-exposure observations such as supernova and afterglows of gamma-ray bursts because the difference could be ignored when comparing the shutter time to the exposure time. The camera records the first line's exposure start time as the images' with its GPS module in short-exposure mode.

To achieve the highest frame rates for searching optical counterparts of fast radio bursts and exoplanets, we tested the maximum frame rates in the region of interest (ROI) mode with different region settings. Our pixel scale is 0.418 arcsec per pixel. The minimally acceptable FoV is 3000 × 1000, with 20 arcmins by 6 arcmins. We tested the maximum frame rate and the longest exposure time at the maximum frame rate for different ROI settings and exposures with an altitude angle higher than 85 degrees on a moonless night

and calculated the limiting magnitude of 5 σ in Table A1. The 50 ms mode of observation could achieve 19.6 fps and magnitude limits down to 12 ~ 13 mag in the g-band compared to the Pan-Starrs DR1 catalogue (PS1,45]). Figure 3 gives a comparison between a 50 ms exposure and a one-second exposure time image.

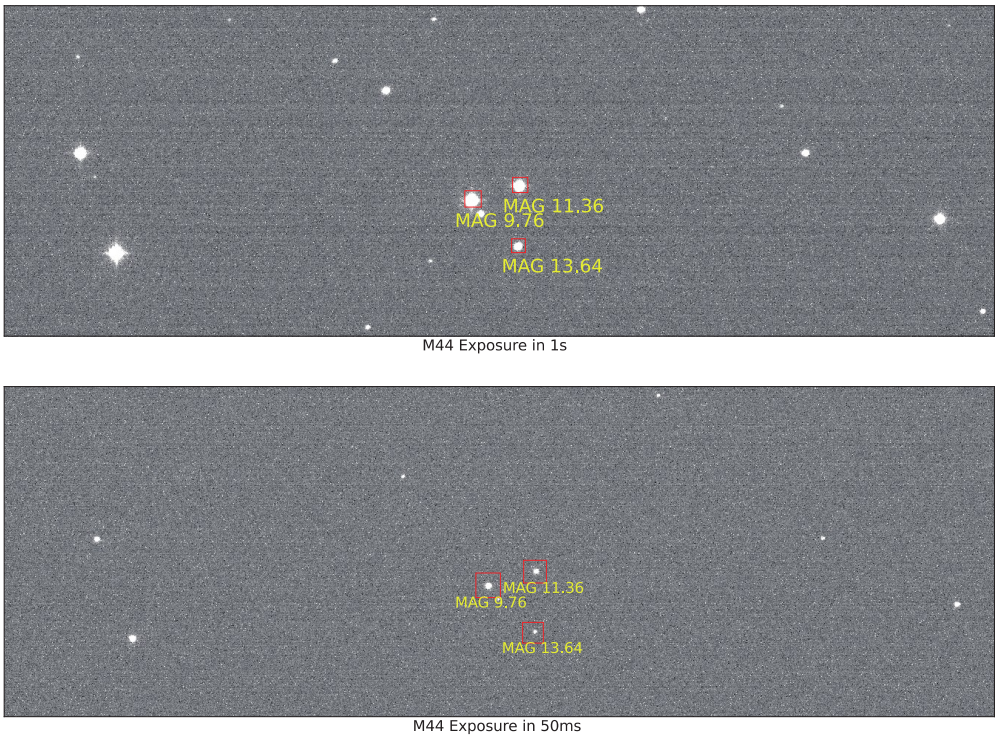

Figure 3. AST3-3 Images for M44 with 1000 ms and 50 ms exposures. The image with a one-second exposure was taken at an altitude of 65 degrees, and the 50 ms exposure image was taken at 78 degrees. The bright stars in the field are circled and marked with their magnitude from the SDSS DR7 catalogue [46].

The telescope is on the third floor of the dome building, and the server computer room is on the ground floor to avoid any heat influence on the environment. To speed up the transfer from a camera to a computer with an image data array, we applied a group of 10 Gigabytes optical fibres instead of USB wire. We use two pairs of 30-meter optical fibres for data transfer and camera control and their backup. These long fibres allow high-performance observation computers to stay away from the dome environment.

2.2. AST3-3 Observation Executor

The AST3-3 observation executes by combining an observation plan scheduler and an observation executor. The observation executor is the main program that runs in the observation server with database interactions, camera control, and telescope connections. More precisely, the executor only follows the observation records in the observation table produced by the scheduler, retrieves the dome status, and updates the camera and telescope control system status to the database. The schedule table in the database is updated instantaneously by the scheduler, which is very convenient for the requests from target-of-opportunity observations. The schedule table contains the target name, globally unique target identifier (the task ID), right ascension, declination, priority, repeat times, and acceptable start and end times of each object.

The executor runs by the straightforward logic shown in Figure 4. For typical observations of flat fields, the executor starts at the Sunsets of $-$ 5 degrees altitude and stops at the Sunrises of $-$ 5 degrees. The observation starts from the opening and connection of the camera, the connection to the telescope control system and the focus engine's enable

and placement. For each observation, the executor selects only the highest priority record with the time condition matches to be executed. The executor checks the observability by the altitude of the object and the distance to the moon with its coordinate by skyfield [47] and astropy [48]. The object altitude should be higher than 30 degrees for each observable object by the limits from the mount and our location.

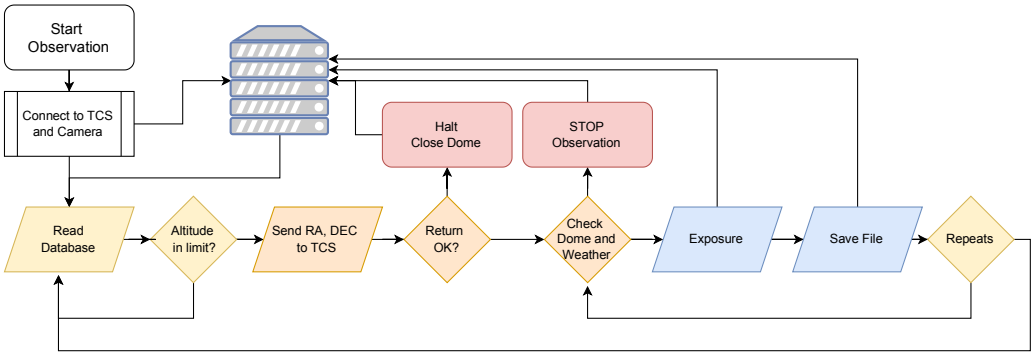

Figure 4AST3-3 Observation Executor workflow. The workflow shows modules with different colours to explain their functionality.

To observe a new sky area, the executor sends the command message with coordinates to the telescope control computer to drift the telescope to the correct position. According to the angle distances, the span of drifting between adjacent points for stabilising is near 10~ 20 s. Before each exposure, the database supplies the dome status to the executor to ensure a fully opened dome. The executor starts the exposure with the camera module after the telescope control system returns information as tracking. To estimate the background immediately, the executor calculates the background estimations for the image centre array directly after the exposure with Python library SEP [49]. The background estimation could also indicate the real-time light pollution from nearby villages and the moon in the observation logging file and the database for image status.

The executor saves the original image data array. Some header information consists of the camera temperature before and after exposure, the camera configuration parameters, the humidity and pressure of the camera, the pointing altitude and azimuth, the telescope encoder positions, the focus status and the background estimations of the image centre as shown in Table A2. While saving, the executor also uploads the header information to the image status database. If it is a multi-image observation, the executor will check the dome and telescope control status before each exposure.

2.3. Weather-Based Protection System

The dry environment of Dome A means that AST3-3 works without dome protection, but it does require a dome for protection when it runs domestically. The dome controller should also be an automatic service for an automatic telescope to avoid humans on guard. The YAHPT group shares their weather station data with us for the protection system of AST3-3. The YAHPT site system has an all-sky camera, weather station and cloud station, providing weather information and critical data.

The protection system retrieves data from the weather station once per minute to define the dome's actions. The local weather station provides temperature, wind speed, humidity and conditional flags for clouds, wind, daylight, and the open and close suggestions of the roof. We retrieve the weather status from the weather station and upload it to our databases by an isolated program every minute. The dome closes when the control program meets either failure of getting weather conditions, or bad weather on the observatory. This pair of guardianship programs would create a disconnection flag into the database to close the dome when the weather data has not been updated for more than five minutes.

The protection procedure works appropriately with two steps: manually or automatically open and close the dome, stop observation, and park the telescope.When the database

shows the weather anomalies or equipment failure, the protection program sends the close dome command to the dome controller via Internet sockets. The weather conditions for observation were restricted to wind speeds lower than ten meters per second and relative humidity lower than 70%. Furthermore, dome closing will not affect the observation directly, and the dome status updates every ten seconds to the database. Before each exposure, the observation program checks the dome status to ensure no exposures while the dome is closed. Most exposures may take 60 s, and dome closing requires a longer time to complete, so the coincidence of exposure and closing does not have much effect.

3. Basic Observation Strategy of AST3-3

The main observational tasks of the time-domain survey are searching for supernovae, asteroids, variable stars, tidal disruption events, active galactic nuclei, and orphan gamma bursts for AST3-3 at Yaoan station. The target of opportunity (ToO) observation requires coordination from other facilities with high-energy transient sources such as gamma-ray bursts, gravitational wave electromagnetic counterparts, and neutrino events. The search area of a time-domain survey should be as large as possible to maximize the candidates. However, the FoV of AST3-3 restricts the observable sky area each night, which requires sky area selections and a scheduler for observation. The AST3-3 scheduler contains both the survey strategy and the follow-up observations for the target of opportunity modules. This section introduces the detailed workflow of the AST3-3 scheduler.

3.1. Transient Survey Strategy

The time-domain survey compares images and catalogues among different observations, which could use fixed sky areas to facilitate the transient searching procedure. By limiting the altitude, the declination range is restricted to -30 degrees to 85 degrees, which allows us to use the g band magnitude data from Pan-Starrs Data Release 1 as the reference for magnitude calibrations.

The sky area grid is slightly smaller than the AST3-3 FoV to overlap the observations on the edge. The sky area grid also matches the Yale Bright star catalogue [50] to avoid bright star influences on the image. Some of the lower galactic latitude sky areas may be influenced by galactic extinctions, and we also calculate the mean galactic extinction [51] for each sky area. Before the time-domain survey, the main observation task for AST3-3 is preparing template images to optimize the image subtraction process in survey and follow-up observations.

As the FoV is not large enough to search the entire observable sky areas, we selected some specific sky areas as the main observation targets to reduce the cadence of the survey and enhance the light curve of observed objects. We choose sky areas with deep-field observations as shown in Table 2, including sky areas from the Cosmic Evolution Survey [52], the Great Observatories Origins Deep Survey (GOODS, [53]), the Galaxy And Mass Assembly survey (GAMA, [54]), the European Large Area ISO Survey (ELAIS, [55]), and the Hyper Suprime-Cam Subaru Strategic Program [56].

We build an automatic scheduler to optimize the survey cadence and the air mass for each image each night before the observation. The observation plan for each night is only considered in optimal weather conditions and a fixed moon phase. The scheduler calculates the twilight flat field plan at first each night with the condition that the flat field should be half-maximum of the full-well value when the solar altitude is between -5 and -10 degrees. It selects the observable sky list by calculating the critical information on the beginning and stop times, including the local sidereal time, planet and moon positions, and solar position.

Within the typical exposure time of 60 s, AST 3-3 could observe about 400∼ 480 images in different seasons. It covers sky areas of about 800∼ 1000 square degrees for single-visit observations. The scheduler schedules the special sky areas for two to three observations per night. We observe special sky areas about one hour before and after transit at the meridian to achieve lower extinction. The selected sky areas are divided into groups of

ten to twenty nearby sky areas for a quick group return visit. It calculates the observation time for each target sky area in the organised sequence. It also estimates the pointing from the last target as the duration for each target with the postman sequence method [57]. The observation sequence is submitted to the database for observation and requested by the executor during the observation time.

Table 2. Special Sky Areas.

Name	R.A.	Dec.	Pointings
GAMA_G02	30.2~ 38.8	−10.25~− 3.72	33
GAMA_G09	129.0~ 141.0	−2~ +3	13
GAMA_G12	174.0~ 186.0	−3~ +2	26
GAMA_G15	211.5~ 223.5	−2~ +3	11
GAMA_G23	339.0~ 351.0	−35~− 30	57
GOODS_N	189.2291	62.2375	8
COSMOS	+150.1191	+2.20583	4
Virgo_Cluster	186.75	12.71	38
ELAIS_N1	242.5041	54.51	1
AEGIS	213~ 217	51.75~ 54.00	4
HSC_SSP	-	-	609

3.2. Automatic Follow Up Strategy

The automatic follow up of essential transients is triggered by other telescopes or satellite facilities from the Internet. The gamma-ray bursts, gravitational wave events, and neutrino events are triggered by the GRB coordinate network (GCN) notices [58]. The CHIME [59] group distributes fast radio bursts coordinates via the VOevent protocol [60], and the Transient Name Sever [61] distributes coordinates via email. We have already built up a system for receiving and analysing these notices. Moreover, the operator checks the reports from The Astronomer's Telegram [62] or the GCN Circular manually.

The centre of the GCN distributes their machine-readable notices via a custom TCP socket protocol to boost the follow-up observations for many telescopes. Since 2012, they have distributed GCN notices in Extensible Markup Language by the protocol suggested by the VOEvent [60] recommendation and allowed anonymous receivers, which could be very flexible for new observation facilities and amateur astronomers.

3.2.1. Gamma-Ray Bursts

The transient parameters include the type, coordinates and errors, trigger time, and attachment information in most cases. Astronomical satellites and ground-based detectors aimed at the high energy transients distribute their notices via GCN notices such as the Swift [63], Fermi [64,65], GECam [66], and IceCube [67] projects. Hence, our scheduler immediately processes this information to the observation list with the predetermined observation strategy.

The strategy gives each type of GCN notice its priority due to the procedure for processing and sending messages. For example, once the SWIFT satellite triggers a gamma-ray burst by the BAT, it sends the notice immediately, and the XRT and UVOT follow. Thus the later notice from UVOT has a more accurate position than the previous coordinate in the notice by BAT. The Gamma-Ray Burst Monitor [64] and Large Area Telescope [65] on Fermi have different coordinate accuracies in a series of real-time and ground-generated notices when we preset separate observation plans.We evaluate and preset the priority in the observation strategy by the coordinate precision in the notice. The preset strategy includes the exposure time, priority and repeats of exposures, which rely on the notice type. Therefore, we have built a flexible and portable system based on applicable type notices as targets.

An independent receiver connects to the GCN server and retrieves all notices automatically. The scheduler reads the packet type and coordinates from the saved notice by the receiver.

If the packet type in Table 3 and the coordinates supplied in the GCN notice seem observable, it would find the matched sky areas and observe these sky areas with the presets' exposure time, priority, and repeats. The GCN network distributes several notices for a typical gamma-ray burst consecutively over several seconds, and the scheduler analyses them separately to avoid procedural conflicts. It transforms each observable GCN notice into an observation request in the database with presets. The priority in Table 3 is a solution for visible object conflicts as the observer program would use the highest priority record in the database.

Table 3. ToO Observation Strategies.

Packet Type	Name	Priority	RadiusErr	Pointings	Repeats	Exposure Time
53	INTEGRAL_WAKEUP	140	10^0	1	30	60 s
54	INTEGRAL_REFINED	141	5^0	1	30	30 s
55	INTEGRAL_OFFLINE	142	3~ 5^0	1	60	60 s
61	SWIFT_BAT_GRB_POS_ACK	131	1-5^0	1	30	30 s
65	SWIFT_FOM_OBS	132	10^0	1	60	30 s
67	SWIFT_XRT_POSITION	134	5^{00}	1	60	60 s
69	SWIFT_XRT_IMAGE	135	5^{00}	1	60	60 s
81	SWIFT_UVOT_POS	137	2^{00}	1	60	60 s
84	SWIFT_BAT_TRANS	133	10^0	1	60	60 s
110	FERMI_GBM_ALERT	100	4~ 10°	~ 20	5	30 s
111	FERMI_GBM_FLT_POS	101	4~ 10°	~ 20	5	30 s
112	FERMI_GBM_GND_POS	102	4~ 10°	~ 40	5	60 s
115	FERMI_GBM_FIN_POS	103	4~ 10°	~ 40	5	60 s
120	FERMI_LAT_POS_INI	110	10–30^0	1	30	60 s
121	FERMI_LAT_POS_UPD	111	10–30^0	1	60	60 s
127	FERMI_LAT_GND	112	10^0	1	60	60 s
173	ICECUBE_ASTROTRACK_GOLD	121	0.2–0.75°	1~ 2	10	60 s
174	ICECUBE_ASTROTRACK_BRONZE	120	0.2–0.75°	1~ 2	10	60 s
-	GECAM_FLIGHT_NOTIC	105	2~ 20°	~ 20	5	60 s
-	GECAM GND-BDS	106	1~ 10°	~ 40	5	60 s

The preset strategy in Table 3 is only used for immediate observation when the telescope observes typically, and the target altitude is higher than 30 degrees. The positional errors in Table 3 for different types of triggers are generated from the website of the GCN system. For some gamma-ray bursts with very large radial error, we are only interested in a part of the sky area that is close to the centre. The priority values are only for the comparison for the observation executor, but are meaningless for the value itself. In Figure 5, we also plot an example for AST3-3 observing the gamma-ray burst from Fermi GBM trigger 669537987 with the probability data from GCN Circular [68].

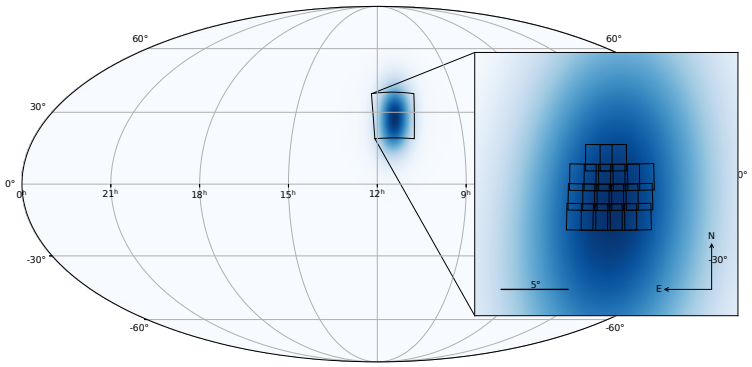

Figure 5. The target of the opportunity observation program produced the observation grids and the observation pointing sequences for GRB 220321A. The trigger number is 669537987, and the probability data from GCN Circular [68].

3.2.2. Gravitational Waves Events

The LIGO-Virgo collaboration detects the signal of gravitational wave events and distributes the trigger notice via the GCN network. Their GCN notices include the GraceID, packet type, alert type, false alarm rate, the probabilities for binary neutron star merger, neutron star - black hole merger and binary black hole merger, and the URL link to the three-dimensional probability sky map of the detected event. They use the BAYESTAR [69] method to create the probability sky map rapidly and supply in the LVC_PRELIMINARY and LVC_INITIAL, LALInference [70] more precisely in LVC_UPDATE GCN notices. Sky maps contain 3D posterior probability distributions represented in the hierarchical equal-area iso-latitude pixelization (HEALPix) array [71]. There would be many follow-up observation reports in the GCN circulars between the preliminary and the update notices, so we observe the LALInference manually and the automatic trigger scheduler only for the BAYESTAR sky maps.

The HEALPix map stores probability data produced by BAYESTAR. We calculate a 3-dimensional probability calculation with the method in [72] and Python example code in [73]. The probability density per unit volume at distance r as Equation (1) in [73] is used here as one component order of priority,

$$\frac{\mathrm{d}P}{\mathrm{d}V} = \rho_i \frac{N_{\mathrm{pix}}}{4\pi} \frac{\hat{N}_i}{\sqrt{2\pi}\hat{\sigma}} \exp - \frac{(r-\hat{\mu})^2}{2\hat{\sigma}} \quad (1)$$

In Equation (1), ρ_i is the 2-dimensional probability in the direction at i-th pixel position, $\hat{\mu}_i$ and $\hat{\sigma}_i$ are the ansatz location and scale parameters, and $\hat{N}_i$ is ansatz normalisation coefficient. The FITS table of the HEALPix map contains N_{pix} records. The probability density $\frac{\mathrm{d}P}{\mathrm{d}V}$ describes the possibility of the gravitational wave event without consideration of the physical parameters of galaxies in the sky area. We optimize our method on follow-up observations with galaxy selections, with the assumption that the short-GRB may be related to some parameter of the host galaxy [74]. During LIGO/Virgo Observation Run 2 and Run 3, there are some methods for sorting galaxies by their physical parameters [75–77]. During the LIGO Observation Run 3, we use the Galaxy List for the Advanced Detector Era [78] as the local galaxy catalogue in the CHanging Event Survey [38] for observation.

AST3-3 prepares to search the optical counterparts of gravitational wave events during LIGO Observation Run 4. We select the GLADE+ [79] catalogue as the local galaxy reference, which provides the estimated binary neutron star merger rate in each galaxy in Gyr^{-1}. Hence, we use the normalized multiplication of $\frac{\mathrm{d}P}{\mathrm{d}V}$ and our estimated star formation rate as the sorting basis for each galaxy.

The scheduler only calculates the sky area of the sum to the top 50% HEALPix pixels, which could avoid the analysis of all pixels and reduce the calculation time. It sums up the normalized results of the galaxies in each sky area and sorts the result as the sequence of

sky areas. We also build a program for retrieving the latest GCN circulars after observation to ensure up-to-date information and unique targets of the event in the whole community for checking the information as soon as possible by the observer.

4. Data Collections

AST3-3 has been well equipped and fully automated for one year and has acquired extensive image data. The image reduction and transient detection pipeline are based on the SFFT algorithm [80]. In this section, we present the observation results with statistics and examples. The observation capability of AST3-3 could be described by the statistics of full-width half-maximum (FWHM), and magnitude limits in different situations. We also present the survey observations of SN2022eyw and the follow-up observations of GRB210420B with their light curves and images.

4.1. Observation Statistics of AST3-3

Since March 2021,AST3-3 has captured more than 40 thousand images that have constructed a good statistical sample. AST3-3 is planned for time-domain observation, which requires the preparation of the templates. For the northern sky, AST3-3 has taken 97% of templates until now. Figure 6 shows the sky grid of AST3-3, and the template coverage is shown in blue points with colours for different template limit magnitudes. The airmass of observation affects the FWHM and the extinctions directly. Based on the stars detected on images by the source extractor [81], we calculated the FWHM for images. Figure 7 shows the FWHM distribution with observation altitudes. The FWHM is centralized to 2.3 arcsec, which aligns with our experience.

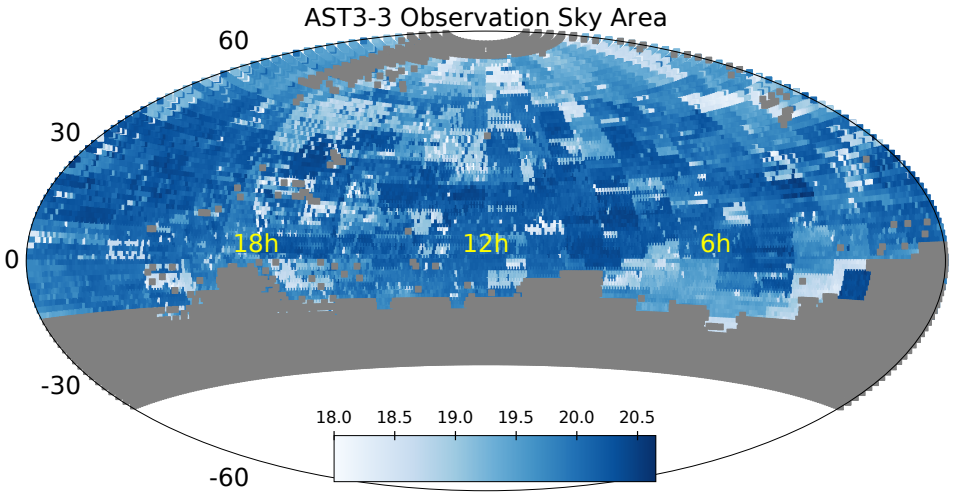

Figure 6. AST3-3 Survey Sky area grids and the magnitude for the prepared template images till now. The magnitude limits are coloured with depth to show that most templates are deeper than 19.0 mags.

The *g*-band used by AST3-3 is strongly influenced by moonlight pollution. There is a significant difference between the limiting magnitudes with and without the moon night in Figure 8. When there is no moon in the observable sky, the magnitude limit depends on the target's altitude. AST3-3 can obtain magnitude limits deeper than 20 mags within a 5σ error, facilitating the search and discovery of transients. Due to the low latitudes of Yaoan Station, sometimes the Moon may have a high altitude, which reduces the magnitude limit to 16 mags or worse.

The differential photometric accuracy is a critical feature for single-band telescopes. We analysed the differential photometry accuracy based on the standard deviation of the light curve for different exposure times. The differential photometry of AST3-3 is performed by the vast [82] to extract the light curves with statistical parameters. Light curve statistics indicate the accuracy of the differential photometry. We plot the scattering point curve

in Figure 9 which shows the standard deviation curve with the magnitude. This curve indicates that the accuracy of AST3-3 is approximately 0.01 mag for 15.6 magnitude stars on a moonless night in Figure 9.

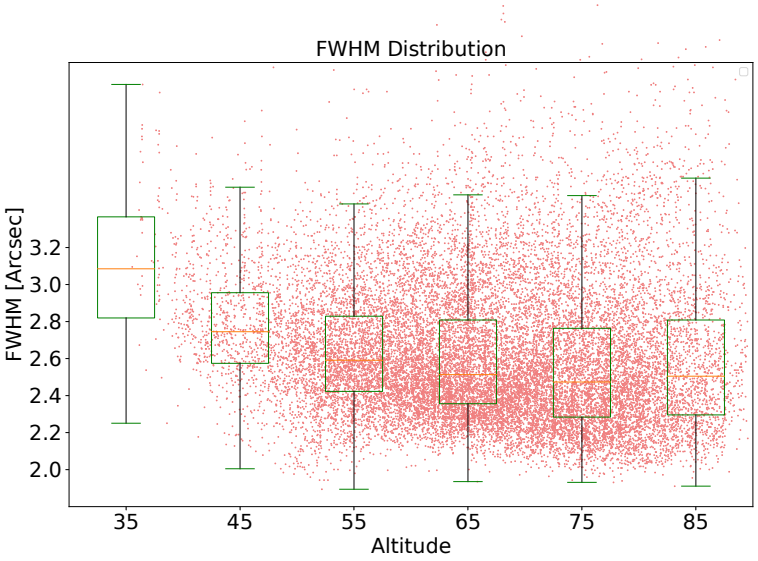

Figure 7. This red points show the AST3-3 statistics for the median FWHM of images in 2021. The box-plot shows the median and standard deviation of altitudes by ten degrees. The FWHM becomes larger when the observation altitude is down to 45 degrees.

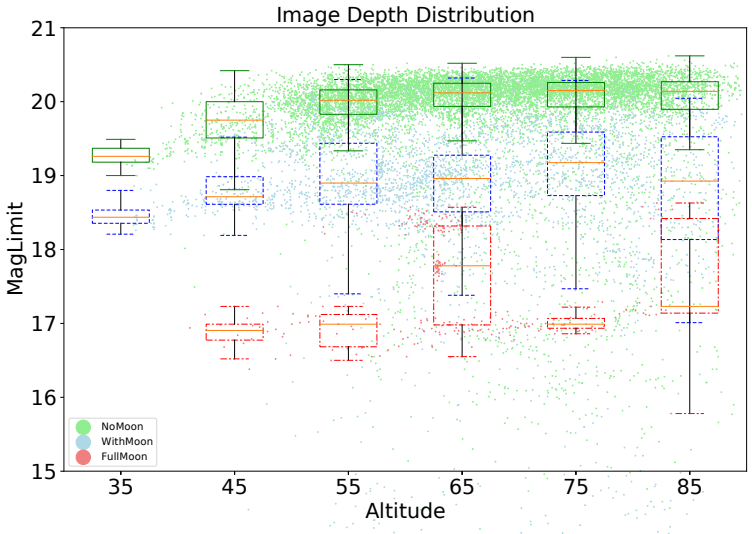

Figure 8. The points shows the magnitude variation with the altitudes in different moon affections. The box-plot shows the median and standard deviation of altitudes by ten degrees.

The image coadd results with GRB 210420B also show the efficiency of the AST3-3 telescope. We coadd ten images to approximately 21 mags and 60 to approximately 21.5 mags with SWarp [83].

4.2. SN 2022eyw Detection by the Time-Domain Survey

Most observation time of AST3-3 is used to construct the templates for the observable sky for transient detections in the time-domain survey and the target of opportunity observation last year. From the beginning of 2022, the AST3-3 survey observes special sky areas. In this subsection, we introduce the AST3-3 observations for SN 2022eyw.

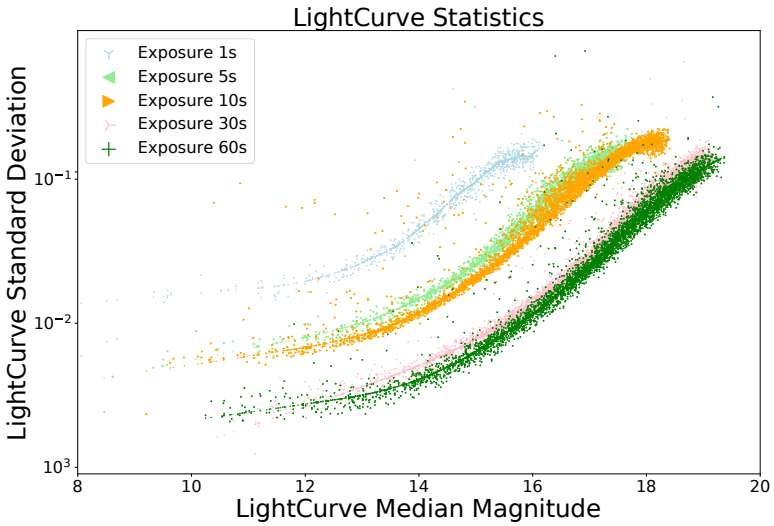

Figure 9. The trends of different colour points show the magnitude statistics in light curves for stars in different exposure times from one second to 60 s. In the centre of each exposure-time group, we use the local regression method to show the major trends.

SN 2022eyw is an i-band magnitude of 19.66 discovered on 22 March 2022, UTC 11:04:36 by Pan-Starrs Survey and reported to the Transient Name Server [84]. The coordinate of SN 2022eyw are a right ascension of 12 h 43 m 59.971 s and a declination of +62 d 19 m 48.30 s. The AST3-3 survey detected this transient at a magnitude of 17.35 in the g-band from the images taken on 24 March 2022, which is part of the GOODS-N sky areas [53]. We observed the same sky area several times before the Pan-Starrs observation on 20 and 21 March 2022, but detected nothing in the combined images as shown in Figure 10.

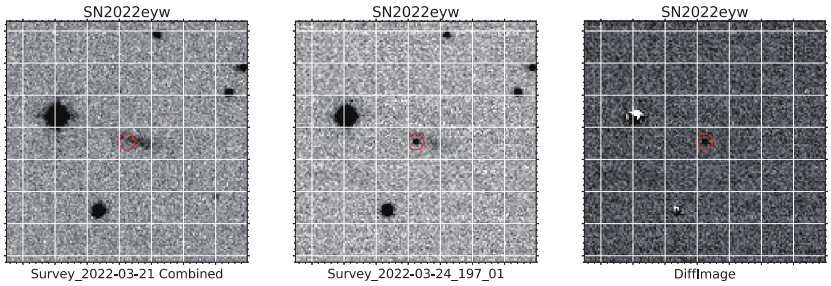

Figure 10. The right image is the combination image from 21 March 2022 at the position of SN 2022eyw with a magnitude limit of 19.26. The middle image is the first discovery image of the SN 2022eyw by AST3-3 on 24 March 2022.The right image is the difference image produced by the transient detection pipeline with SFFT [80].

Tagchi et al. [85] and Balcon [86] took the spectrum for SN 2022eyw and confirmed it as a rare type Iax supernova. The spectrum result was also confirmed by the Liverpool Telescope on 31 March 2022 by Fulton et al. [87]. From 24 March to 30 March 2022, AST3-3 acquired 28 observation images in this sky area. We plot the photometry points with data from both AST3-3 and TNS as shown in Figure 11.

4.3. Follow-Up Observation of Gamma-Ray Burst 210420B

The Swift group triggered a gamma-ray burst GRB 210420B at the position RA (J2000) of 16 h 57 m 17.39 s and Dec (J2000) of +42 d 34 m 10.2 s with an uncertainty of 3.6 arcsec [88]. GRB 210420B is a long GRB with T90 (15–350 keV) of 158.8 ± 29.5 s [88], with a equivalent isotropic energy of 7.7×10^{51} erg for the redshift of 1.4. And the Swift XRT data shows a power-law decay with an index of α of 2.23 and a break at T+425 s to an index of α of 1.13 [89]. We began the follow-up observation with AST3-3 on 20 April 2021 at 20:07

UTC, approximately one hour and a half after the BAT trigger. We took 67 consecutive, valid images using a fixed 60 s exposure and found the object within the XRT position during this observation. The optical afterglow of GRB210420B is shown in Figure 12 with coaddition to enhance the contrast of the image. There are several oscillating spikes in the AST3-3 data, which may imply the existence of voids and jumps in the ambient density of this burst [90,91]. The combined optical data shows that the optical flux decreases slowly around 10^4 s, and even re-brightens at 2×10^4 s. This chromatic evolution in the X-ray and the optical band indicates that a simple traditional forward shock model is not sufficient to account for all the observations [92]. The late-time optical behaviour could be understood by invoking a new emission component emerging from a reverse shock produced by the additional energy injection processes [93,94], which will be presented in another following work.

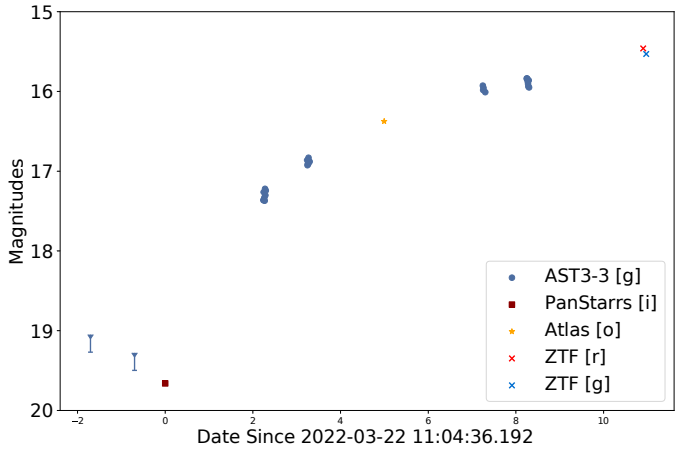

Figure 11. The light curve for SN 2022eyw combines photometry data from Pan-Starrs, ATLAS and ZTF. AST3-3 observation gives the magnitude limit before the report from Pan-Starrs. The filter o for ATLAS is orange-ATLAS. All the TNS data is taken from TNS Website. https://www.wis-tns.org/object/2022eyw (accessed on 19 May 2022).

The light curve of our observation is shown in Figure 13 with the seconds from UT 18:34:37 20 April 2020 [95]. Our result is consistent with reports from MASTER [96], Hankasalmi [97], and the BOOTES [98]. Within the candidate position [97], we detected a source with 18.6 mags on 20 April 2021 20:07:30 and 19.13 mags on 20 April 2021 21:42:43. We use the [99] method for the calculation of the magnitude zero-point. The limiting magnitude was around 20.5 magnitude during the observation, and we reported this information in the GCN Circular.

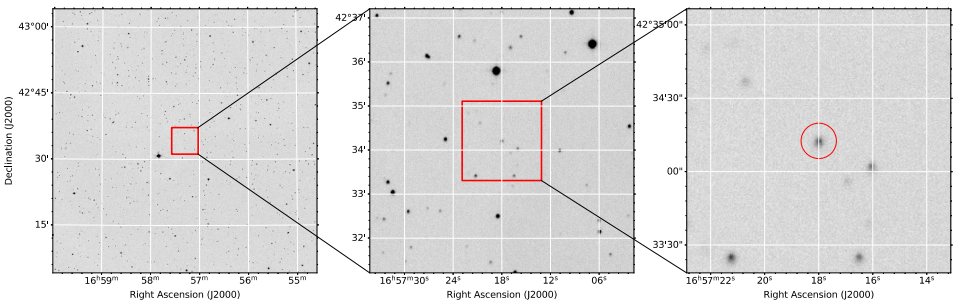

Figure 12. The three panel shows the different zoom scale for the GRB 210420B images. The **left panel** shows a 1-degree FoV image of the GRB 210420B. The **middle panel** shows the 0.1-degree FoV of the GRB 210420B. Moreover, the **right panel** shows the two arcmin FoV of the GRB 210420B.

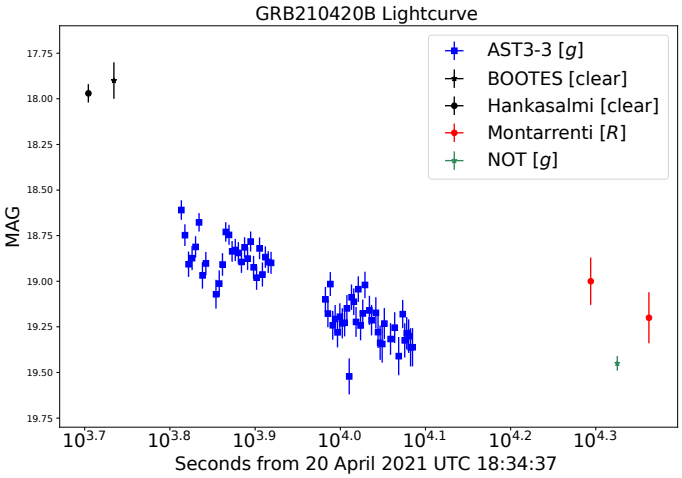

Figure 13. This image shows the light curve of the GRB 210420B. The light curve combines data from AST3-3, BOOTES [98], Hankasalmi [97], Montarrenti [100] and NOT [101].

5. Conclusions

This paper describes the basic information of the AST3-3 telescope, the observation strategy, and some of the preliminary results. Now, we have enabled AST3-3 to enter the data acquisition phase formally. With the protection and network system, this telescope can fully automate the observation of every visual record in the database. The AST3-3 telescope is a 50/68 cm aperture telescope with FoV of $1.65^{\circ} \times 1.23^{\circ}$ in Yaoan, Yunnan. The main advantage of AST3-3 in the era of time-domain astronomy is supported by its fully automated observation scheduling and data pipeline system. Observations start and stop automatically by weather conditions, and we only need manual checks for very special alarms due to unusual problems. We have thousands of templates for the time-domain survey. Time-domain surveys and template shooting were the main tasks.

However, the short-exposure observations still require more testing on short-period variable stars to test the differential photometry accuracy. Automatic follow-ups with the source coordinates from GCN Circular and Astronomers' Telegram are still another problem. The manual recognition of the contents reduces the flexibility and extends the response time. We may need more profound research.

Author Contributions: Conceptualization, L.W. and X.W.; methodology, T.S. and X.L.; software, T.S., X.L. and H.W. (Huihui Wang); validation, L.H. and K.M.; resources, X.L., H.W. (Haikun Wen), B.G., F.D., S.Y., L.L., Y.L., X.Y., X.H., Z.L. and C.L.; data curation, T.S., M.H. and L.H.; writing—original draft preparation, T.S. and K.M.; writing—review and editing, X.L., L.H. and Z.H.; visualization, T.S. and L.H.; supervision, X.W.; project administration, X.Y., Z.Z., L.W. and X.W.; funding acquisition, X.W. All authors have read and agreed to the published version of the manuscript.

Funding: This work is partially supported by the National Natural Science Foundation of China (Grant Nos. 11725314, 12041306, 11903019, 12173062), the Major Science and Technology Project of Qinghai Province (2019-ZJ-A10). The research is also partly supported by the Operation, Maintenance and Upgrading Fund for Astronomical Telescopes and Facility Instruments, budgeted by the Ministry of Finance of China (MOF) and administrated by the Chinese Academy of Sciences (CAS). Tianrui Sun thanks to the China Scholarship Council (CSC) for funding his PhD scholarship (202006340174).

Institutional Review Board Statement: Not applicable.

Informed Consent Statement: Not applicable.

Data Availability Statement: Not applicable.

Acknowledgments: The AST3-3 team would like to express their sincere thanks to the staff of the Yaoan observation station. The AST3-3 team would like to thank the Yaoan High Precision Telescope group for their kindly shared weather data and follow-up observation resources. The authors

thank Jinjun Geng for his wonderful analysis of the GRB 210420B data. The authors also thank Yu-Song Cao for his kindly grammatical suggestions on our draft. The authors are also grateful to anonymous referees whose opinion has significantly improved this manuscript. This research has made use of data and services provided by the International Astronomical Union's Minor Planet Center. This work has made use of data from the European Space Agency (ESA) mission *Gaia* (https://www.cosmos.esa.int/gaia (accessed on 19 May 2022)), processed by the *Gaia* Data Processing and Analysis Consortium (DPAC, https://www.cosmos.esa.int/web/gaia/dpac/consortium (accessed on 19 May 2022)). Funding for the DPAC has been provided by national institutions, in particular the institutions participating in the *Gaia* Multilateral Agreement. This research has made use of NASA's Astrophysics Data System Bibliographic Services. Softwares: This research made use of Astropy, http://www.astropy.org (accessed on 19 May 2022) a community-developed core Python package for Astronomy [102,103]. The python packages: pyephem [104], skyfield [47], matplotlib [105], scipy [106], statsmodels [107], and sep [49].

Conflicts of Interest: The authors declare no conflict of interest.

Appendix A

Table A1. Frame Rate For QHY411 with Optical Fibre.

Resolution	Frame Rates at 16 Bit	Max Exposure Time	Magnitude Limit
Full Frame	-	1 s	16.59
Full Frame	2.0 FPS	500 ms	15.73
5374 Lines	3.9 FPS	500 ms	15.73
3000 Lines	7.2 FPS	135 ms	14.61
2000 Lines	10 FPS	100 ms	13.63
1000 Lines	20 FPS	50 ms	11.74

Table A2. AST3-3 Header in Observation fits file.

Card Name	Typical Value	Comment
CAMERA	'QHY411MERIS'	camera ID
EXPOSURE	60	exposure
MODE	4	read out mode
FILTER	'*g*'	fixed
DATE-OBS	'2021-06-20T17:56:51.304'	time before exposure
DATE-END	'2021-06-20T17:57:53.496'	time after exposure
SKY	923.79	center background
SKYSIG	12.206	center background RMS
TEMP1	−27.9	CMOS temperature before exposure
TEMP2	−27.0	CMOS temperature after exposure
PWMSET	255.0	cooler PWM setting
COOLER	−50.0	cooler target temperature
GAMMA	1.0	gamma value
OFFSET	50.0	offset of coms camera
RA	279.752319	target right ascension
DEC	10.0	target declination
ALTITUDE	74.48	altitude
AZIMUTH	178.3	azimuth
SKYIDX	'1839 + 1000'	target name
ENCRA	'− 0.518577'	encoder right ascension
ENCDEC	'9.808846'	encode declination
FOCPOS	'12.090'	focus position
HA	'359.481423'	hour angle of target

References

1. Price, P.A.; Magnier, E.A.Pan-STARRS PSF-Matching for Subtraction and Stacking*arXiv* **2019**, arXiv:1901.09999.
2. Bellm, E. The Zwicky Transient Facility. In Proceedings of the Third Hot-Wiring the Transient Universe Workshop, Santa Fe, NM, USA, 13–15 November 2013; pp. 27–33

3. Bellm, E.C.; Kulkarni, S.R.; Graham, M.J.; Dekany, R.; Smith, R.M.; Riddle, R.; Masci, F.J.; Helou, G.; Prince, T.A.; Adams, S.M.; et al. The Zwicky Transient Facility: System Overview, Performance, and First Results. *Publ. Astron. Soc. Pac.* **2019**, *131*, 018002. [CrossRef]
4. Tonry, J.L.; Denneau, L.; Heinze, A.N.; Stalder, B.; Smith, K.W.; Smartt, S.J.; Stubbs, C.W.; Weiland, H.J.; Rest, A. ATLAS: A High-cadence All-sky Survey System. *Publ. Astron. Soc. Pac.* **2018**, *130*, 064505. [CrossRef]
5. Gompertz, B.P.; Cutter, R.; Steeghs, D.; Galloway, D.K.; Lyman, J.; Ulaczyk, K.; Dyer, M.J.; Ackley, K.; Dhillon, V.S.; O'Brien, P.T.; et al. Searching for electromagnetic counterparts to gravitational-wave merger events with the prototype Gravitational-Wave Optical Transient Observer (GOTO-4). *Mon. Not. RAS* **2020**, *497*, 726–738. [CrossRef]
6. Scalzo, R.A.; Yuan, F.; Childress, M.J.; Möller, A.; Schmidt, B.P.; Tucker, B.E.; Zhang, B.R.; Onken, C.A.; Wolf, C.; Astier, P.; et al. The SkyMapper Transient Survey. *Publ. Astron. Soc. Aust.* **2017**, *34*, e030. [CrossRef]
7. Becerra, R.L.; Dichiara, S.; Watson, A.M.; Troja, E.; Butler, N.R.; Pereyra, M.; Moreno Méndez, E.; De Colle, F.; Lee, W.H.; Kutyrev, A.S.; et al. DDOTI observations of gravitational-wave sources discovered in O3. *Mon. Not. RAS* **2021**, *507*, 1401–1420. [CrossRef]
8. Walkowicz, L. The Large Synoptic Survey Telescope. In Proceedings of the SALT Science Conference 2015 (SSC2015), Stellenbosch Institute of Advanced Study, South Africa, 1–5 June 2015; p. 20.
9. Zhang, T.M.; Wang, X.F.; Chen, J.C.; Zhang, J.J.; Zhou, L.; Li, W.X.; Liu, Q.; Mo, J.; Zhang, K.C.; Yao, X.Y.; et al. The THU-NAOC transient survey: The performance and results from the first year. *Res. Astron. Astrophys.* **2015**, *15*, 215–224. [CrossRef]
10. Zhang, J.C.; Wang, X.F.; Mo, J.; Xi, G.B.; Lin, J.; Jiang, X.J.; Zhang, X.M.; Li, W.X.; Yan, S.Y.; Chen, Z.H.; et al. The Tsinghua University-Ma Huateng Telescopes for Survey: Overview and Performance of the System. *Publ. Astron. Soc. Pac.* **2020**, *132*, 125001. [CrossRef]
11. Wang, X.; Zhao, H.B.; Xia, Y.; Lu, H.; Li, B. CNEOST Control Software System. *Acta Astron. Sin.* **2015**, *56*, 178–188. [CrossRef]
12. Yang, X.; Shang, Z.; Hu, K.; Hu, Y.; Ma, B.; Wang, Y.; Cao, Z.; Ashley, M.C.B.; Wang, W. Cloud cover and aurora contamination at dome A in 2017 from KLCAM. *Mon. Not. RAS* **2021**, *501*, 3614–3620. [CrossRef]
13. Kenyon, S.L.; Storey, J.W.V. A Review of Optical Sky Brightness and Extinction at Dome C, Antarctica. *Publ. Astron. Soc. Pac.* **2006**, *118*, 489–502. [CrossRef]
14. Storey, J.W.V. Astronomy from Antarctica. *Antarct. Sci.* **2005**, *17*, 555. [CrossRef]
15. Lawrence, J.S.; Ashley, M.C.B.; Burton, M.G.; Cui, X.; Everett, J.R.; Indermuehle, B.T.; Kenyon, S.L.; Luong-Van, D.; Moore, A.M.; Storey, J.W.V.; et al. Site testing Dome A, Antarctica. In Proceedings of Ground-based and Airborne Telescopes, Orlando, FL, USA, 24–31 May 2006; Volume 6267.
16. Ashley, M.C.B. Site characteristics of the high Antarctic plateau. In Proceedings of the International Astronomical Union, Nanjing, China, 24 August 2012; Volume 8. Symposium S288: Astrophysics from Antarctica. [CrossRef]
17. Storey, J.W.V. Introduction to the Antarctic Plateau. *Chin. Astron. Astrophys.* **2007**, *31*, 98–100. [CrossRef]
18. Shang, Z. Astronomy from Dome A in Antarctica. *Res. Astron. Astrophys.* **2020**, *20*, 168. [CrossRef]
19. Zou, H.; Zhou, X. The i-band Sky brightness and Transparency at Dome A, Antarctica. *arXiv* **2011**, arXiv:1101.2362.
20. Yang, Y.; Moore, A.M.; Krisciunas, K.; Wang, L.; Ashley, M.C.B.; Fu, J.; Brown, P.J.; Cui, X.; Feng, L.L.; Gong, X.; et al. Optical Sky Brightness and Transparency during the Winter Season at Dome A Antarctica from the Gattini-All-Sky Camera. *Astron. J.* **2017**, *154*, 6. [CrossRef]
21. Hu, Y.; Shang, Z.; Ashley, M.C.B.; Bonner, C.S.; Hu, K.; Liu, Q.; Li, Y.; Ma, B.; Wang, L.; Wen, H. Meteorological Data for the Astronomical Site at Dome A, Antarctica. *Publ. Astron. Soc. Pac.* **2014**, *126*, 868. [CrossRef]
22. Zhou, X.; Ashley, M.C.B.; Cui, X.; Feng, L.; Gong, X.; Hu, J.; Jiang, Z.; Kulesa, C.A.; Lawrence, J.S.; Liu, G.; et al. Progress and Results from the Chinese Small Telescope ARray (CSTAR). In Proceedings of the International Astronomical Union, Nanjing, China, 24 August 2012; Volume 8. Symposium S288: Astrophysics from Antarctica. [CrossRef]
23. Li, X.; Wang, D.; Xu, L.; Zhao, J.; Du, F.; Zhang, Y. Control system for the first three Antarctic Survey Telescopes (AST3-1). In Proceedings of the Ground-Based and Airborne Telescopes IV, Amsterdam, The Netherlands, 1–6 July 2012; Volume 8444.
24. Li, X.; Yuan, X.; Gu, B.; Yang, S.; Li, Z.; Du, F. Chinese Antarctic Astronomical Optical Telescopes. *Rev. Mex. Astron. Astrofis. Conf. Ser.* **2019**, *51*, 135–138.
25. Wang, L.; Macri, L.M.; Ma, B.; Wang, L.F.; Ashley, M.C.B.; Cui, X.; Du, F.J.; Fu, J.N.; Feng, L.L.; Gong, X.; et al. Stellar variability from Dome A, Antarctica. *EPJ Web Conf.* **2017**, *152*, 02010. [CrossRef]
26. Huang, T.J.; Sun, T.R.; Hu, L.; Ning, Z.J.; Wu, X.F.; Wang, L.F.; Wang, X.H. An Automatic Method for Detecting Transients and Variable Sources in AST3 Survey Based on Image Subtraction and Random Forest. *Chin. Astron. Astrophys.* **2020**, *44*, 41–60. [CrossRef]
27. Liang, E.S.; Zhang, H.; Yu, Z.; Yang, M.; Zhou, J.l.; Ashley, M.C.B.; Cui, X.; Du, F.; Fu, J.; Gong, X.; et al. Exoplanets in the Antarctic Sky. III. Stellar Flares Found by AST3-II (CHESPA) within the Southern CVZ of TESS. *Astron. J.* **2020**, *159*, 201. [CrossRef]
28. Zhang, H.; Yu, Z.; Liang, E.; Yang, M.; Ashley, M.C.B.; Cui, X.; Du, F.; Fu, J.; Gong, X.; Gu, B.; et al. Exoplanets in the Antarctic Sky. I. The First Data Release of AST3-II (CHESPA) and New Found Variables within the Southern CVZ of TESS. *Astrophys. J. Suppl.* **2019**, *240*, 16. [CrossRef]
29. Zhang, H.; Yu, Z.; Liang, E.; Yang, M.; Ashley, M.C.B.; Cui, X.; Du, F.; Fu, J.; Gong, X.; Gu, B.; et al. Exoplanets in the Antarctic Sky. II. 116 Transiting Exoplanet Candidates Found by AST3-II (CHESPA) within the Southern CVZ of TESS. *Astrophys. J. Suppl.* **2019**, *240*, 17. [CrossRef]

30. Hu, L.; Wu, X.; Andreoni, I.; Ashley, M.C.B.; Cooke, J.; Cui, X.; Du, F.; Dai, Z.; Gu, B.; Hu, Y.; et al. Optical observations of LIGO source GW 170817 by the Antarctic Survey Telescopes at Dome A, Antarctica. *Sci. Bull.* **2017**, *62*, 1433–1438. [CrossRef]
31. Andreoni, I.; Ackley, K.; Cooke, J.; Acharyya, A.; Allison, J.R.; Anderson, G.E.; Ashley, M.C.B.; Baade, D.; Bailes, M.; Bannister, K.; et al. Follow Up of GW170817 and Its Electromagnetic Counterpart by Australian-Led Observing Programmes. *Publ. Astron. Soc. Aust.* **2017**, *34*, e069. [CrossRef]
32. Ma, B.; Hu, Y.; Shang, Z.; Hu, K.; Wang, Y.; Yang, X.; Ashley, M.C.B.; Yuan, X.; Wang, L. Automation of the AST3 optical sky survey from Dome A, Antarctica. *Mon. Not. RAS* **2020**, *496*, 2768–2775. [CrossRef]
33. Yuan, X.; Cui, X.; Wang, L.; Gu, B.; Du, F.; Li, Z.; Yang, S.; Li, X.; Lu, H.; Wen, H.; et al. The Antarctic Survey Telescopes AST3 and the AST3-NIR. *IAU Gen. Assem.* **2015**, *29*, 2256923.
34. Burton, M.G.; Zheng, J.; Mould, J.; Cooke, J.; Ireland, M.; Uddin, S.A.; Zhang, H.; Yuan, X.; Lawrence, J.; Ashley, M.C.B.; et al. Scientific Goals of the Kunlun Infrared Sky Survey (KISS). *Publ. Astron. Soc. Aust.* **2016**, *33*, e047. [CrossRef]
35. Yuan, X.; Su, D.Q. Optical system of the Three Antarctic Survey Telescopes. *Mon. Not. RAS* **2012**, *424*, 23–30. [CrossRef]
36. Zheng, J.R.; Churilov, V.; Content, R.; Lawrence, J.; Gu, B.; Lu, H.; Wen, H.; Yuan, X. Optical system design of the AST3-NIR camera. In Proceedings of the Ground-Based and Airborne Instrumentation for Astronomy VII, Austin, TX, USA, 10–15 June 2018.
37. Farr, B.; LIGO Scientific Collaboration; Virgo Collaboration. The Latest Results from the LIGO-Virgo O3 Observing Run. In Proceedings of the American Astronomical Society Meeting Abstracts #235, Honolulu, HI, USA, 4–8 January 2020; Volume 235, p. 119.02.
38. Zhang, C.; Ping, Y.; Zhao, C. CHES: A Rapid All-Sky Survey System for SSA. In Proceedings of the The Advanced Maui Optical and Space Surveillance Technologies Conference, Wailea, Maui, HI, USA, 11–14 September 2018.
39. Castro-Tirado, A.J. Robotic Astronomy and the BOOTES Network of Robotic Telescopes. *Acta Polytech.* **2011**, *51*, 16. [CrossRef]
40. Boer, M.; Klotz, A.; Atteia, J.L.; Buchholtz, G.; Daigne, F.; Eysseric, J.; Goldoni, P.; Jean, P.; Lecavelier Des Etangs, A.; Lopez, M.; et al. The Gamma-Ray Burst Hunt at La Silla the TAROT-S Very Fast Moving Telescope. *Messenger* **2003**, *113*, 45–48.
41. Watson, A.M.; Cuevas Cardona, S.; Alvarez Nuñez, L.C.; Ángeles, F.; Becerra-Godínez, R.L.; Chapa, O.; Farah, A.S.; Fuentes-Fernández, J.; Figueroa, L.; Langarica Lebre, R.; et al. COATLI: An all-sky robotic optical imager with 0.3 arcsec image quality. In Proceedings of the Ground-Based and Airborne Instrumentation for Astronomy VI, Edinburgh, UK, 26 June–1 July 2016.
42. Becerra, R.L.; Watson, A.M.; Fraija, N.; Butler, N.R.; Lee, W.H.; Troja, E.; Román-Zúñiga, C.G.; Kutyrev, A.S.; Álvarez Nuñez, L.C.; Ángeles, F.; et al. Late Central-engine Activity in GRB 180205A. *Astrophys. J.* **2019**, *872*, 118. [CrossRef]
43. Lipunov, V.M.; Krylov, A.V.; Kornilov, V.G.; Borisov, G.V.; Kuvshinov, D.A.; Belinsky, A.A.; Kuznetsov, M.V.; Potanin, S.A.; Antipov, G.A.; Tyurina, N.V.; et al. MASTER: The Mobile Astronomical System of Telescope-Robots. *Astron. Nachr.* **2004**, *325*, 580–582. [CrossRef]
44. Yuan, Y.; Li, F.; Fu, Y.; Ren, S. New precise positions in 2013–2019 and a catalog of ground-based astrometric observations of 11 Neptunian satellites (1847–2019) based on Gaia-DR2. *Astron. Astrophys.* **2021**, *645*, A48. [CrossRef]
45. Flewelling, H. Pan-STARRS Data Release 1. In Proceedings of the American Astronomical Society Meeting Abstracts #229, Grapevine, TX, USA, 3–7 January 2017; Volume 229, p. 237.
46. Abazajian, K.N.; Adelman-McCarthy, J.K.; Agüeros, M.A.; Allam, S.S.; Allende Prieto, C.; An, D.; Anderson, K.S.J.; Anderson, S.F.; Annis, J.; Bahcall, N.A.; et al. The Seventh Data Release of the Sloan Digital Sky Survey. *Astrophys. J. Suppl.* **2009**, *182*, 543–558. [CrossRef]
47. Rhodes, B. Skyfield: High Precision Research-Grade Positions for Planets and Earth Satellites Generator. Avaliable online: http://ascl.net/1907.024 (accessed on 21 May 2022).
48. Greenfield, P.; Robitaille, T.; Tollerud, E.; Aldcroft, T.; Barbary, K.; Barrett, P.; Bray, E.; Crighton, N.; Conley, A.; Conseil, S.; et al. Astropy: Community Python Library for Astronomy. Available online: http://ascl.net/1304.002 (accessed on 21 May 2022).
49. Barbary, K. SEP: Source Extractor as a library. *J. Open Source Softw.* **2016**, *1*, 58. [CrossRef]
50. Warren, W.H.J.; Hoffleit, D. The Bright Star Catalogue, 5th ed. Available online: https://ui.adsabs.harvard.edu/abs/1987BAAS...19..733W/abstract (accessed on 21 May 2022).
51. Schlegel, D.J.; Finkbeiner, D.P.; Davis, M. Maps of Dust Infrared Emission for Use in Estimation of Reddening and Cosmic Microwave Background Radiation Foregrounds. *Astrophys. J.* **1998**, *500*, 525–553. [CrossRef]
52. Scoville, N.; Aussel, H.; Brusa, M.; Capak, P.; Carollo, C.M.; Elvis, M.; Giavalisco, M.; Guzzo, L.; Hasinger, G.; Impey, C.; et al. The Cosmic Evolution Survey (COSMOS): Overview. *Astrophys. J. Suppl.* **2007**, *172*, 1–8. [CrossRef]
53. Giavalisco, M.; Ferguson, H.C.; Koekemoer, A.M.; Dickinson, M.; Alexander, D.M.; Bauer, F.E.; Bergeron, J.; Biagetti, C.; Brandt, W.N.; Casertano, S.; et al. The Great Observatories Origins Deep Survey: Initial Results from Optical and Near-Infrared Imaging. *Astrophys. J. Lett.* **2004**, *600*, L93–L98. [CrossRef]
54. Liske, J.; Baldry, I.K.; Driver, S.P.; Tuffs, R.J.; Alpaslan, M.; Andrae, E.; Brough, S.; Cluver, M.E.; Grootes, M.W.; Gunawardhana, M.L.P.; et al. Galaxy And Mass Assembly (GAMA): End of survey report and data release 2. *Mon. Not. RAS* **2015**, *452*, 2087–2126. [CrossRef]
55. Oliver, S.; Rowan-Robinson, M.; Alexander, D.M.; Almaini, O.; Balcells, M.; Baker, A.C.; Barcons, X.; Barden, M.; Bellas-Velidis, I.; Cabrera-Guerra, F.; et al. The European Large Area ISO Survey—I. Goals, definition and observations. *Mon. Not. RAS* **2000**, *316*, 749–767. [CrossRef]

56. Aihara, H.; AlSayyad, Y.; Ando, M.; Armstrong, R.; Bosch, J.; Egami, E.; Furusawa, H.; Furusawa, J.; Harasawa, S.; Harikane, Y.; et al. Third data release of the Hyper Suprime-Cam Subaru Strategic Program. *Publ. Astron. Soc. Jpn.* **2022**, *74*, 247–272. [CrossRef]
57. Sömen, O.; Emeç, S.; Yilmaz, M.; Akkaya, G. An Overview of Chinese Postman Problem. In Proceedings of the 3rd International Conference on Advanced Engineering Technologies, Duhok, Kurdistan Region-Iraq, 2–4 April 2019.
58. Barthelmy, S. GCN and VOEvent: A status report. *Astron. Nachr.* **2008**, *329*, 340. [CrossRef]
59. Kaspi, V.M.; CHIME/FRB Collaboration. The CHIME Fast Radio Burst Project. In Proceedings of the American Astronomical Society Meeting Abstracts #229, Grapevine, TX, USA, 3–7 January 2017; Volume 229, p. 242.
60. Swinbank, J.D.; Allan, A.; Denny, R.B. VOEvent Transport Protocol Version 2.0. IVOA Recommendation 20 March 2017. Available online: https://ui.adsabs.harvard.edu/abs/2017ivoa.spec.0320S/abstract (accessed on 21 May 2022).
61. Gal-Yam, A. The TNS Alert System. Available online: https://baas.aas.org/pub/2021n1i423p05 (accessed on 21 May 2022).
62. Rutledge, R.E. The Astronomer's Telegram: A Web-based Short-Notice Publication System for the Professional Astronomical Community. *Publ. Astron. Soc. Pac.* **1998**, *110*, 754–756. [CrossRef]
63. Moss, M.J.; Evans, P.A.; Gronwall, C.; Gropp, J.D.; Kennea, J.A.; Page, K.L.; Sbarufatti, B.; Neil Gehrels Swift Observatory Team. GRB 210420B: Swift detection of a burst. *GRB Coord. Netw.* **2021**, *29844*, 1.
64. Meegan, C.; Lichti, G.; Bhat, P.N.; Bissaldi, E.; Briggs, M.S.; Connaughton, V.; Diehl, R.; Fishman, G.; Greiner, J.; Hoover, A.S.; et al. The Fermi Gamma-ray Burst Monitor. *Astrophys. J.* **2009**, *702*, 791–804. [CrossRef]
65. Atwood, W.B.; Abdo, A.A.; Ackermann, M.; Althouse, W.; Anderson, B.; Axelsson, M.; Baldini, L.; Ballet, J.; Band, D.L.; Barbiellini, G.; et al. The Large Area Telescope on the Fermi Gamma-Ray Space Telescope Mission. *Astrophys. J.* **2009**, *697*, 1071–1102. [CrossRef]
66. Li, Y.; Wen, X.; Sun, X.; Liu, X.; Liang, X.; Guo, D.; Peng, W.; Gong, K.; Li, G.; Wang, H.; et al. The GECAM and its payload. *Sci. Sin. Phys. Mech. Astron.* **2020**, *50*, 129508. [CrossRef]
67. Clark, B.A.; Clark, B.A.; IceCube-Gen2 Collaboration. The IceCube-Gen2 Neutrino Observatory. *J. Instrum.* **2021**, *16*, C10007. [CrossRef]
68. Fermi GBM Team. GRB 220321A: Fermi GBM Final Localization. *GRB Coord. Netw.* **2022**, *31777*, 1.
69. Singer, L.P.; Price, L.R. Rapid Bayesian position reconstruction for gravitational-wave transients. *Phys. Rev. D* **2016**, *93*, 024013. [CrossRef]
70. Veitch, J.; Raymond, V.; Farr, B.; Farr, W.; Graff, P.; Vitale, S.; Aylott, B.; Blackburn, K.; Christensen, N.; Coughlin, M.; et al. Parameter estimation for compact binaries with ground-based gravitational-wave observations using the LALInference software library. *Phys. Rev. D* **2015**, *91*, 042003. [CrossRef]
71. Górski, K.M.; Hivon, E.; Banday, A.J.; Wandelt, B.D.; Hansen, F.K.; Reinecke, M.; Bartelmann, M. HEALPix: A Framework for High-Resolution Discretization and Fast Analysis of Data Distributed on the Sphere. *Astrophys. J.* **2005**, *622*, 759–771. [CrossRef]
72. Singer, L.P.; Chen, H.Y.; Holz, D.E.; Farr, W.M.; Price, L.R.; Raymond, V.; Cenko, S.B.; Gehrels, N.; Cannizzo, J.; Kasliwal, M.M.; et al. Going the Distance: Mapping Host Galaxies of LIGO and Virgo Sources in Three Dimensions Using Local Cosmography and Targeted Follow-up. *Astrophys. J. Lett.* **2016**, *829*, L15. [CrossRef]
73. Singer, L.P.; Chen, H.Y.; Holz, D.E.; Farr, W.M.; Price, L.R.; Raymond, V.; Cenko, S.B.; Gehrels, N.; Cannizzo, J.; Kasliwal, M.M.; et al. Supplement: "Going the Distance: Mapping Host Galaxies of LIGO and Virgo Sources in Three Dimensions Using Local Cosmography and Targeted Follow-up" (2016, ApJL, 829, L15). *Astrophys. J. Suppl.* **2016**, *226*, 10. [CrossRef]
74. Berger, E. Short-Duration Gamma-Ray Bursts. *Annu. Rev. Astron. Astrophys.* **2014**, *52*, 43–105. [CrossRef]
75. Arcavi, I.; McCully, C.; Hosseinzadeh, G.; Howell, D.A.; Vasylyev, S.; Poznanski, D.; Zaltzman, M.; Maoz, D.; Singer, L.; Valenti, S.; et al. Optical Follow-up of Gravitational-wave Events with Las Cumbres Observatory. *Astrophys. J. Lett.* **2017**, *848*, L33. [CrossRef]
76. Fan, X.; Messenger, C.; Heng, I.S. A Bayesian Approach to Multi-messenger Astronomy: Identification of Gravitational-wave Host Galaxies. *Astrophys. J.* **2014**, *795*, 43. [CrossRef]
77. Fan, X.; Messenger, C.; Heng, I.S. Enhancing Gravitational Wave Astronomy with Galaxy Catalogues. In *Gravitational Wave Astrophysics*; Springer: Cham, Switzerland, 2015; Volume 40, p. 35. [CrossRef]
78. Dálya, G.; Galgóczi, G.; Dobos, L.; Frei, Z.; Heng, I.S.; Macas, R.; Messenger, C.; Raffai, P.; de Souza, R.S. GLADE: A galaxy catalogue for multimessenger searches in the advanced gravitational-wave detector era. *Mon. Not. RAS* **2018**, *479*, 2374–2381. [CrossRef]
79. Dálya, G.; Díaz, R.; Bouchet, F.R.; Frei, Z.; Jasche, J.; Lavaux, G.; Macas, R.; Mukherjee, S.; Pálfi, M.; de Souza, R.S.; et al. GLADE+: An Extended Galaxy Catalogue for Multimessenger Searches with Advanced Gravitational-wave Detectors. *arXiv* **2021**, arXiv:2110.06184.
80. Hu, L.; Wang, L.; Chen, X. Image Subtraction in Fourier Space. *arXiv* **2021**, arXiv:2109.09334.
81. Bertin, E.; Arnouts, S. SExtractor: Software for source extraction. *Astron. Astrophys. Suppl.* **1996**, *117*, 393–404. [CrossRef]
82. Sokolovsky, K.V.; Lebedev, A.A. VaST: A variability search toolkit. *Astron. Comput.* **2018**, *22*, 28–47. [CrossRef]
83. Bertin, E. SWarp: Resampling and Co-Adding FITS Images Together. 2010. Available online: http://ascl.net/1010.068 (accessed on 21 May 2022).

84. Chambers, K.C.; Boer, T.D.; Bulger, J.; Fairlamb, J.; Huber, M.; Lin, C.C.; Lowe, T.; Magnier, E.; Schultz, A.; Wainscoat, R.J.; et al. Pan-STARRS Transient Discovery Report for 2022-03-23. Available online: https://www.wis-tns.org/ads/TNSTR-2022-762 (accessed on 21 May 2022).
85. Tagchi, K.; Namekata, K.; Kawabata, M.; Nakaoka, T.; Yamanaka, M. Transient Classification Report for 2022-03-25. Available online: https://ui.adsabs.harvard.edu/abs/2022TNSCR.783....1T/abstract (accessed on 21 May 2022).
86. Balcon, C. Transient Classification Report for 2022-03-26. Available online: https://ui.adsabs.harvard.edu/abs/2022TNSCR.792....1B/abstract (accessed on 21 May 2022).
87. Fulton, M.; Srivastav, S.; Smartt, S.J.; Smith, K.W.; Young, D.R.; Sim, S.A.; Gillanders, J.; Moore, C. TUB Transient Classification Report for 2022-03-31. Available online: https://www.wis-tns.org/ads/TNSCR-2022-833 (accessed on 21 May 2022).
88. Stamatikos, M.; Barthelmy, S.D.; Cummings, J.R.; Krimm, H.A.; Laha, S.; Lien, A.Y.; Markwardt, C.B.; Palmer, D.M.; Sakamoto, T.; Ukwatta, T.N. GRB 210420B: Swift-BAT refined analysis. *GRB Coord. Netw.* **2021**, *29879*, 1.
89. Osborne, J.P.; Capalbi, M.; Perri, M.; D'Elia, V.; Gropp, J.D.; Kennea, J.A.; Tohuvavohu, A.; Page, K.L.; Beardmore, A.P.; Moss, M.J.; et al. GRB 210420B: Swift-XRT refined Analysis. *GRB Coord. Netw.* **2021**, *29876*, 1.
90. Uhm, Z.L.; Zhang, B. Dynamics and Afterglow Light Curves of Gamma-Ray Burst Blast Waves Encountering a Density Bump or Void. *Astrophys. J.* **2014**, *789*, 39. [CrossRef]
91. Geng, J.J.; Wu, X.F.; Li, L.; Huang, Y.F.; Dai, Z.G. Revisiting the Emission from Relativistic Blast Waves in a Density-jump Medium. *Astrophys. J.* **2014**, *792*, 31. [CrossRef]
92. Sari, R.; Piran, T.; Narayan, R. Spectra and Light Curves of Gamma-Ray Burst Afterglows. *Astrophys. J. Lett.* **1998**, *497*, L17–L20. [CrossRef]
93. Geng, J.J.; Wu, X.F.; Huang, Y.F.; Yu, Y.B. Delayed Energy Injection Model for Gamma-Ray Burst Afterglows. *Astrophys. J.* **2013**, *779*, 28. [CrossRef]
94. Geng, J.J.; Wu, X.F.; Huang, Y.F.; Li, L.; Dai, Z.G. Imprints of Electron-Positron Winds on the Multiwavelength Afterglows of Gamma-ray Bursts. *Astrophys. J.* **2016**, *825*, 107. [CrossRef]
95. Lien, A.Y.; Moss, M.J.; Tohuvavohu, A.; Neil Gehrels Swift Observatory Team. GRB 210420B: Update on the BAT trigger time. *GRB Coord. Netw.* **2021**, *29854*, 1.
96. Lipunov, V.; Kornilov, V.; Gorbovskoy, E.; Chasovnikov, A.; Balanutsa, P.; Vladimirov, V.; Kuznetsov, A.; Vlasenko, D.; Tiurina, N.; Gorbunov, I.; et al. GRB 210420B: MASTER optical counterpart detection. *GRB Coord. Netw.* **2021**, *29845*, 1.
97. Oksanen, A. GRB 210420B: Optical observations. *GRB Coord. Netw.* **2021**, *29846*, 1.
98. Hu, Y.D.; Sun, T.R.; Fernandez-Garcia, E.; Castro-Tirado, A.J.; Caballero-Garcia, M.D.; Castro Tirado, M.A.; Perez del Pulgar, C.; Castellon, A.; Carrasco, I.; Guziy, S.; et al. GRB 210420B: BOOTES-4/MET optical afterglow detection. *GRB Coord. Netw.* **2021**, *29847*, 1.
99. Mommert, M.; Moskovitz, N.; Trilling, D.E. PHOTOMETRYPIPELINE—An Automated Pipeline for Calibrated Photometry. In Proceedings of the AAS/Division for Planetary Sciences Meeting, Pasadena, CA, USA, 16–21 October 2016.
100. Leonini, S.; Conti, M.; Rosi, P.; Tinjaca Ramirez, L.M. GRB 210420B: Montarrenti Observatory optical afterglow detection. *GRB Coord. Netw.* **2021**, *29851*, 1.
101. de Ugarte Postigo, A.; Malesani, D.B.; Knudstrup, E. GRB 210420B: Multiband photometry from NOT. *GRB Coord. Netw.* **2021**, *29852*, 1.
102. Astropy Collaboration; Robitaille, T.P.; Tollerud, E.J.; Greenfield, P.; Droettboom, M.; Bray, E.; Aldcroft, T.; Davis, M.; Ginsburg, A.; Price-Whelan, A.M.; et al. Astropy: A community Python package for astronomy. *Astron. Astrophys.* **2013**, *558*, A33. [CrossRef]
103. Astropy Collaboration; Price-Whelan, A.M.; Sip˝ocz, B.M.; Günther, H.M.; Lim, P.L.; Crawford, S.M.; Conseil, S.; Shupe, D.L.; Craig, M.W.; Dencheva, N.; et al. The Astropy Project: Building an Open-science Project and Status of the v2.0 Core Package. *Astron. J.* **2018**, *156*, 123. [CrossRef]
104. Rhodes, B.C. PyEphem: Astronomical Ephemeris for Python. Available online: http://ascl.net/1112.014 (accessed on 21 May 2022).
105. Hunter, J.D. Matplotlib: A 2D Graphics Environment. *Comput. Sci. Eng.* **2007**, *9*, 90–95. [CrossRef]
106. Jones, E.; Oliphant, T.; Peterson, P. SciPy: Open Source Scientific Tools for Python. 2001. Available online: https://scipy.org/ (accessed on 21 May 2022).
107. Seabold, S.; Perktold, J. Statsmodels: Econometric and statistical modeling with python. In Proceedings of the 9th Python in Science Conference, Austin, TX, USA, 28 June–3 July 2010.